High-pressure behavior of $Ba(OH)_2$: Phase transitions and bulk modulus

Alexandra Friedrich,* Martin Kunz,† and Ronald Miletich‡
Laboratorium für Kristallographie, ETH Zentrum, Sonneggstrasse 5, CH-8092 Zürich, Switzerland

Philip Pattison
SNBL at ESRF, BP220, F-38043 Grenoble Cedex, France
and Institut de Cristallographie, Université de Lausanne, BSP - Dorigny, CH-1015 Lausanne, Switzerland

(Received 7 February 2002; revised manuscript received 8 August 2002; published 11 December 2002)

The high-pressure behavior of both β- and α-$Ba(OH)_2$ was investigated by *in situ* powder synchrotron x-ray diffraction. Pressures up to 13 GPa were generated using a diamond-anvil cell. At least one phase transition was detected in β-$Ba(OH)_2$ [$P2_1/n$; $a=9.3396(2)$, $b=7.8550(2)$, $c=6.7267(2)$ Å, $\beta=95.607(2)°$ at 0.95 GPa], indicated by the appearance of an additional low-angle peak. The high-pressure β_2 phase [$P2_1/c$; $a=11.6632(8)$, $b=7.6684(5)$, $c=10.7785(7)$ Å, $\beta=108.881(5)°$ at 5.40 GPa] is characterized by a doubling of the unit-cell volume. Bulk moduli were determined for β-$Ba(OH)_2$ with $K_0=40(1)$ GPa (K' fixed to 6) and for β_2-$Ba(OH)_2$ with $K_0=60(4)$ GPa (K' fixed to 6). There are indications for two other phase transitions between 8 and 10 GPa. Compressing α-$Ba(OH)_2$ produces new diffraction patterns, which cannot be interpreted unambiguously. Upon pressure release down to 0.3 GPa, the β_2 phase is recovered.

DOI: 10.1103/PhysRevB.66.214103 PACS number(s): 61.50.Ks, 64.70.Kb, 81.30.Hd

I. INTRODUCTION

A central question in numerous recent studies on hydrous materials is the potential of high pressure to strengthen or even induce hydrogen bonds and the concomitant influence on the physical properties of these materials. A comprehensive understanding of the mutual influence of hydrogen bonds on structural and physical properties requires the combined investigation of bulk properties (i.e., compressibility, thermal conductivity) and structural features as a function of external variables (chemistry, temperature, pressure). It is the complementary nature of these combined studies which enable the distinction of chemical effects from pressure and temperature effects on hydrogen bonding.[1]

High-pressure investigations were previously performed on alkaline-earth hydroxides $A(OH)_2$ (A=Mg,Ca) (Refs. 2–10) and transition-metal hydroxides $T(OH)_2$ (T=Mn, Fe, Co, Ni, Cd),[1,11,12] both on hydrogenated and deuterated samples. These compounds have as a common feature a layered structure related to the CdI_2 type. The H atoms are situated between adjacent XO_6 ($X=A,T$) octahedral sheets. The comparison of elastic properties revealed a difference between the bulk moduli of hydroxides containing main-group elements and transition metals, respectively.[1] Structural studies at high pressure on Mn and β-Co hydroxides revealed a strengthening of the hydrogen bonds leading to a D-site disorder.[1] For brucite [$Mg(OH)_2$], the existence of a phase transition, which was suggested to be induced by changes in the hydrogen bond geometry,[13] is still uncertain. In contrast, the postulated high-pressure phase of portlandite [$Ca(OH)_2$-II] (Ref. 14) was confirmed and its structure solved.[15] Subsequent work aimed at unraveling the influence of Ca/Mg replacement on the elastic properties in hydroxides[16] and at the location of deuterium atoms in $Ca(OD)_2$-II.[17] This issue has also been addressed on the basis of a computational approach.[18] The framework of the monoclinic high-pressure structure ($P2_1/c$) is isostructural to that of EuI_2. The topology of this structure type is very similar to the one of $Sr(OD)_2$ at ambient conditions.[19] This confirms the hypothesis that replacing Mg^{2+} and Ca^{2+} with larger cations such as Sr^{2+} or Ba^{2+} can provide some insight into the structural behavior of brucite or portlandite under high pressure,[20] which was our motivation to study barium hydroxide at high pressure.

At ambient conditions, $Ba(OH)_2$ occurs in two modifications, the low-temperature β phase and the high-temperature α phase, which crystallizes at temperatures above 526(2) K.[21] The α phase is quenchable and hence can be retrieved as a metastable phase at room temperature. The crystal structures of α- and β-$Ba(OH)_2$ were previously reported both on hydrogenated and deuterated samples.[22–24] The temperature-dependent behavior of both polymorphs was investigated by powder neutron diffraction,[25] which revealed a new metastable low-temperature polymorph of α-$Ba(OD)_2$.

II. EXPERIMENT

Pure powder of the β modification of barium hydroxide, β-$Ba(OH)_2$, was synthesized using $Ba(OH)_2 \cdot 8H_2O$ as the starting material. This was filled in a corundum crucible and placed in a quartz-glass tube under a nitrogen atmosphere, where it was slowly heated to 373 K for dehydration. Water vapor was removed by several evacuation cycles. The α modification of barium hydroxide, α-$Ba(OH)_2$, was obtained by heating a sample of the β phase up to 573 K with subsequent quenching to room temperature.

The sample chamber [150(5) μm in diameter] was drilled into tungsten gaskets (pre-indented to a thickness of 60–70 μm) using an electroerosion drilling machine. Pressure was generated with an ETH-designed[26] diamond-anvil cell (DAC) using liquid argon as a pressure-transmitting medium. The complete loading process was performed without exposing the CO_2- and H_2O-sensitive samples to air or water at any instance.

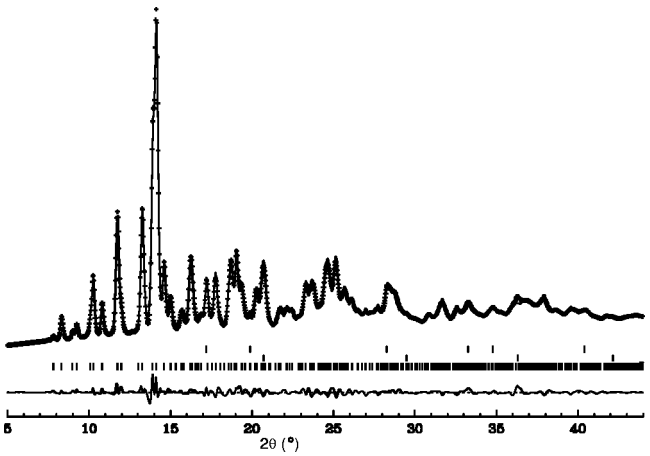

FIG. 1. Observed (crosses) and calculated (line) powder-diffraction patterns, and difference curve of β_2-Ba$(OH)_2$ at 6.2 GPa. Peak positions are given for Ar (top), W (center), and β-Ba$(OH)_2$ (bottom).

In situ high-pressure synchrotron x-ray powder-diffraction data were collected for both materials at steps of approximately 1–2 GPa up to 13 GPa at the Swiss-Norwegian Beamline (BM1A) of the European Synchrotron Radiation Facility (Grenoble, France). Two angle-dispersive powder-diffraction patterns were collected at every pressure point using a MAR345 image-plate system. The first pattern was recorded at a sample-to-detector distance of 170 mm ($2\theta_{max}=24°$), while the second exposure was at a distance of 380 mm ($2\theta_{max}=45°$). The exposure time ranged from 60 s to 300 s depending on the distance and the cell loading. A wavelength of 0.8 Å was used. The absorption edge of the tungsten gaskets near 0.8 Å helped to minimize contamination of the sample signal by parasitic diffraction from the gasket. For two loadings, deviatoric stress at the highest pressure was reduced by placing the entire pressure cell in a furnace and heating the whole assembly to ~378 K during one hour. Pressures were determined by means of the laser-induced ruby-fluorescence technique before and after each exposure.

Full powder-diffraction images were processed and integrated using FIT2D.[27] Diffraction spots of solid argon and diamond reflections were masked and thus excluded from integration. Rietveld refinements were carried out with GSAS.[28] Starting values for the refinements of β-Ba$(OH)_2$ and α-Ba$(OH)_2$ were those reported by Friedrich, Kunz, and Suard.[25] Lattice parameters, atomic fractional coordinates, and isotropic displacement parameters for the barium atoms were varied. The displacement parameters of the oxygen atoms were fixed to $U_{iso}=0.02$ Å^2. In addition, background coefficients of a shifted Chebyshev function,[28] scale factor, and a pseudo-Voigt profile function were refined. For some of the data sets, additional diffracting phases, such as the pressure-cell components (tungsten and beryllium) and the solidified pressure-transmitting medium (argon), had to be included in the refinement as well, Fig. 1.

III. RESULTS AND DISCUSSION

Unit-cell parameters and the final discrepancy factors are summarized in Table I. Atomic fractional coordinates and isotropic displacement parameters are given in Table II.

A. Structural results

1. Crystal structures of β- and α-Ba$(OH)_2$

The β phase of Ba$(OH)_2$ crystallizes in space group $P2_1/n$. There are two symmetrically different barium sites, Ba1 coordinated by eight [8], and Ba2 surrounded by seven [7+1] oxygen atoms, Fig. 2(a). The face-linked polyhedra form serrated double chains along the *b* axis. These chains are connected via edges along the *a* axis and form interstitials within a sheet, which are occupied by H atoms. The sheets are interconnected via polyhedral edges or corners. Hydrogen bonds exist within the cavities.

The α phase of Ba$(OH)_2$ crystallizes in space group $Pnma$. The crystal structure includes three symmetrically distinct barium sites, Ba1 coordinated by [8], Ba2 by [7+1], and Ba3 by [9] hydroxyl groups, Fig. 2(b). An additional nine-coordinated interstitial site is occupied by hydrogen atoms. More detailed information is given in Friedrich, Kunz, and Suard.[25]

2. Pressure-induced changes of the β-Ba$(OH)_2$ powder-diffraction pattern

At the closing pressure of 0.95 GPa unit-cell parameters of $a=9.3396(2)$, $b=7.8550(2)$, $c=6.7267(2)$ Å, and $\beta=95.607(2)°$ were refined for β-Ba$(OH)_2$. All reflections could be indexed and refined in space group $P2_1/n$, except those from the tungsten gasket or the beryllium backing plates. Above 1.2 GPa, additional spotty lines appeared. They were identified as diffraction lines from solid argon, which was used as a pressure-transmitting medium.

The powder-diffraction pattern of β-Ba$(OH)_2$ undergoes various significant changes upon increasing pressure. We explain these changes by the occurrence of at least one phase transition. Between 4.9 GPa and 9 GPa a new low-angle peak grows continuously at $d\sim6.15$ Å ($2\theta\sim7.5°$), Fig. 3. Since this peak cannot be explained by the β phase it indicates a phase transition to a new β_2 phase with a larger unit cell. Automatic indexing using TREOR (Ref. 29) gives a monoclinic unit cell with $a=11.6632(8)$, $b=7.6684(5)$, $c=10.7785(7)$ Å, and $\beta=108.881(5)°$ at $P=5.40$ GPa. The β unit cell transforms to the β_2 cell through the transformation matrix

$$\begin{pmatrix} \bar{1} & 0 & 1 \\ 0 & \bar{1} & 0 \\ 1 & 0 & 1 \end{pmatrix}.$$

The $\boldsymbol{a}$ and $\boldsymbol{c}$ unit vectors of the β_2 cell thus relate to the $[\bar{1}01]$ and $[101]$ directions of the β cell, respectively, Fig. 4. This corresponds to a doubling of the β_2 unit cell relative to the β unit-cell volume. The indexing can account for all reflections assuming space group $P2_1/c$. The phase transi-

TABLE I. Unit-cell parameters and refinement values of $Ba(OH)_2$ as a function of pressure. $R_{wp}=\sqrt{\Sigma w(I_o-I_c)^2/\Sigma w(I_o^2)}$, $R_p=\Sigma|I_o-I_c|/\Sigma I_o$, and $R(F^2)=\Sigma|F_o^2-SF_c^2|/\Sigma|F_o^2|$, where $w=$ weight, and $S=$ scale factor.

P (GPa)	a (Å)	b (Å)	c (Å)	$\beta(°)$	V(Å^3)	V(Å^3) Ar	$R(F^2)$	R_{wp}	R_p
				β-$Ba(OH)_2$					
0.0001[a]	9.4094(3)	7.9155(2)	6.7745(2)	95.813(2)	501.97(3)		7.35	4.67	3.51
0.95(5)	9.3396(2)	7.8550(2)	6.7267(2)	95.607(2)	491.13(2)		3.90	2.55	1.79
1.30(5)	9.3050(4)	7.8197(3)	6.6990(3)	95.503(3)	485.19(3)	129.37(3)	3.21	2.97	2.13
2.00(5)	9.2789(5)	7.7962(4)	6.6761(4)	95.415(4)	480.80(4)	123.16(2)	2.67	3.38	2.34
2.50(5)	9.2436(6)	7.7681(5)	6.6487(5)	95.285(2)	475.39(6)	116.60(3)	2.87	2.56	1.83
3.3(2)	9.2169(7)	7.7405(5)	6.6223(5)	95.201(5)	470.51(6)	112.42(2)	3.44	3.40	2.40
				β_2-$Ba(OH)_2$					
0.34(5)	12.0951(7)	7.8891(5)	11.0013(6)	108.569(4)	995.1(1)		6.41	3.88	2.72
4.9(2)	9.1512(9)	7.6821(7)	6.5575(6)	94.930(7)	459.29(7)	103.92(3)	3.22	3.70	2.65
	11.715(1)	7.6880(7)	10.799(1)	108.828(8)	920.5(1)		6.15	4.54	3.14
5.40(5)	9.1245(6)	7.6597(5)	6.5293(5)	94.785(5)	454.75(5)	100.91(3)	3.59	3.12	2.26
	11.6632(8)	7.6684(5)	10.7785(7)	108.881(5)	912.1(1)		5.90	3.03	2.27
5.80(5)	11.655(1)	7.660(1)	10.785(1)	108.95(1)	910.7(2)	100.33(5)	4.43	5.76	3.84
6.20(5)	9.1200(7)	7.6562(6)	6.5173(6)	94.703(8)	453.54(5)	99.33(5)	3.03	4.11	3.04
	11.6338(9)	7.6555(7)	10.7641(9)	108.967(8)	906.6(1)		6.89	4.55	3.27
6.80(5)	11.587(1)	7.650(1)	10.759(2)	109.10(1)	901.3(2)	97.2(1)	6.91	5.22	3.83
7.30(5)	11.5585(9)	7.6277(7)	10.7324(9)	109.082(8)	894.2(1)	95.57(4)	7.29	4.27	2.99
7.70(5)	11.536(1)	7.6302(9)	10.732(1)	109.22(1)	892.0(2)	94.17(5)	5.35	3.71	2.64
8.10(5)	11.5202(7)	7.6199(5)	10.7239(8)	109.187(6)	889.1(1)	93.84(4)	4.65	3.63	2.66
8.40(5)	11.469(2)	7.582(1)	10.658(2)	109.12(1)	875.6(2)	93.84(6)	4.48	3.13	2.23
				α-$Ba(OH)_2$					
0.0001[a]	11.0111(6)	16.4994(8)	7.0954(4)	90			12.88	7.40	5.52

[a]Capillary measurements.

tion does thus not change point group $2/m$. However, since the unit cell of the β_2 phase is double the size of the β cell, symmetry operations are diluted by a factor of 2, Fig. 4. The unit cell of the β_2 phase is therefore a ''klassengleiche'' supercell of the β cell.

Above 9.0 GPa, a possible new β_3 phase is evidenced by the appearance of three additional weak peaks at d values of 7.32, 6.90, and 6.47 Å ($2\theta=6.26°, 6.65°, 7.09°$), respectively, Fig. 3. At the same pressure, the relative intensities of several peaks change significantly, which is a strong indication that these new observed peaks are indeed due to a phase transformation. The powder-diffraction pattern undergoes yet another significant change at 10.1 GPa where the intensity of the strong reflection around $d=4.41$ Å ($2\theta=10.4°$ in Fig. 3) shows a dramatic decrease. This new feature remains also after heating, thus relaxing some of the deviatoric stress, which causes a significant decrease of the peak width. Attempts to index the diffraction patterns recorded at pressures above 9 GPa with TREOR,[29] ITO,[30] or DICVOL (Ref. 31) were not successful. There are four possible factors contributing to this failure: (i) The resolution of powder-diffraction patterns at high pressure is generally lower than what is optimal to index complex structures, (ii) the unit cells of the new phases are larger in size (additional low-angle peaks) and thus more complex, (iii) the symmetry of the new phases may be lowered to one of the subgroups of $P2_1/c$ such as $P2_1$, Pc or $P\bar{1}$ adding further complexity, and (iv) anisotropic peak shifts might occur due to nonhydrostatic pressure conditions. It cannot be entirely excluded that the various proposed new phases are in fact only one single phase, where the new appearing peaks at 9.0 GPa are simply too weak to be detected at lower pressures. We consider this as rather unlikely mainly in view of the strong changes in relative intensities within the diffraction patterns parallel to the appearance of new reflections, Fig. 3. The β_2 phase, on the other hand, seems indeed to represent a new polytype despite the fact that it is evidenced by only a single peak. The already rather low symmetry and thus high number of peaks make it very difficult to detect any new peaks other than the lowest-angle ones. In fact the proposed β_2 supercell is the smallest possible unit cell explaining all of the observed peaks.

3. Structural evolution of β- and β_2-$Ba(OH)_2$ with pressure

Structural refinement of the low-symmetry compounds against the high-pressure powder-diffraction data turned out to be difficult. This is because of three reasons: (i) Our data are limited in the accessible 2θ range, due to the use of the DAC; (ii) the pressure-generating environment induces additional diffraction lines, which partly overlap with the sample signal, Fig. 1; (iii) high-pressure data show peak broadening due to nonhydrostatic conditions. These factors made it impossible to refine a structure in the β_2 model against the data above 4 GPa. Additional constraints had to be introduced in order to improve stability and convergence of the least-squares refinement. As a possible constraint we assumed that the symmetry-reducing distortion is small and therefore

TABLE II. Atom positions and atomic displacement parameters of β-$Ba(OH)_2$.

	x	y	z	U_{iso}
		0.0001 GPa		
Ba1	0.6023(3)	0.6401(3)	0.2498(4)	0.02
Ba2	0.1810(2)	0.5484(3)	0.2168(3)	0.02
O1	0.881(2)	0.491(2)	0.190(2)	0.025
O2	0.416(2)	0.358(2)	0.164(3)	0.025
O3	0.607(2)	0.337(2)	0.476(3)	0.025
O4	0.153(2)	0.287(2)	0.467(3)	0.025
		0.95 GPa		
Ba1	0.6029(3)	0.6407(2)	0.2515(4)	0.0049(9)
Ba2	0.1803(2)	0.5479(2)	0.2153(3)	0.0080(8)
O1	0.873(1)	0.469(2)	0.172(2)	0.005(6)
O2	0.410(1)	0.358(2)	0.150(2)	0.003(6)
O3	0.602(2)	0.343(2)	0.501(2)	0.016(6)
O4	0.167(2)	0.295(2)	0.462(3)	0.03
		1.3 GPa		
Ba1	0.6033(3)	0.6417(3)	0.2496(4)	0.010(1)
Ba2	0.1794(2)	0.5481(2)	0.2171(3)	0.0085(8)
O1	0.873(2)	0.476(2)	0.176(2)	0.02
O2	0.414(2)	0.367(2)	0.152(2)	0.02
O3	0.611(2)	0.344(2)	0.505(3)	0.02
O4	0.165(2)	0.295(2)	0.463(3)	0.02
		2.0 GPa		
Ba1	0.6043(3)	0.6426(3)	0.2486(4)	0.012(1)
Ba2	0.1792(3)	0.5487(3)	0.2165(4)	0.010(1)
O1	0.872(2)	0.478(2)	0.188(3)	0.02
O2	0.415(2)	0.368(2)	0.154(3)	0.02
O3	0.608(2)	0.342(2)	0.508(3)	0.02
O4	0.163(2)	0.295(3)	0.459(3)	0.02
		2.5 GPa		
Ba1	0.6037(3)	0.6436(3)	0.2492(4)	0.008(1)
Ba2	0.1796(2)	0.5487(2)	0.2177(3)	0.0094(8)
O1	0.871(2)	0.469(2)	0.173(2)	0.02
O2	0.412(2)	0.366(2)	0.159(2)	0.02
O3	0.612(2)	0.343(2)	0.498(3)	0.02
O4	0.164(2)	0.291(2)	0.460(2)	0.02
		3.3 GPa		
Ba1	0.6049(4)	0.6442(4)	0.2479(5)	0.013(1)
Ba2	0.1786(3)	0.5471(3)	0.2164(4)	0.014(1)
O1	0.871(2)	0.475(3)	0.187(3)	0.02
O2	0.421(2)	0.368(3)	0.160(3)	0.02
O3	0.616(2)	0.339(3)	0.503(4)	0.02
O4	0.168(2)	0.297(3)	0.457(3)	0.02
		4.9 GPa		
Ba1	0.6058(4)	0.6461(4)	0.2462(6)	0.015(2)
Ba2	0.1793(4)	0.5470(4)	0.2162(5)	0.013(1)
O1	0.874(3)	0.482(3)	0.195(4)	0.02
O2	0.417(3)	0.369(3)	0.165(4)	0.02
O3	0.615(3)	0.330(3)	0.489(4)	0.02
O4	0.166(3)	0.304(4)	0.455(4)	0.02
		5.4 GPa		
Ba1	0.6054(4)	0.6467(4)	0.2483(5)	0.015(2)
Ba2	0.1772(3)	0.5487(3)	0.2169(4)	0.012(1)
O1	0.865(2)	0.467(3)	0.185(3)	0.02
O2	0.416(3)	0.379(3)	0.169(4)	0.02
O3	0.623(3)	0.326(3)	0.492(4)	0.02
O4	0.155(2)	0.297(3)	0.455(4)	0.02
		6.2 GPa		
Ba1	0.6057(5)	0.6474(5)	0.2488(7)	0.009(2)
Ba2	0.1764(4)	0.5484(4)	0.2186(6)	0.005(1)
O1	0.870(3)	0.479(3)	0.195(4)	0.02
O2	0.418(3)	0.379(4)	0.170(5)	0.02
O3	0.630(4)	0.332(4)	0.489(5)	0.02
O4	0.166(3)	0.286(4)	0.456(5)	0.02

could be neglected by using the structural model of the β phase. This procedure allows to follow some major structural trends such as averaged bond distances also in the β_2 phase. The assumption becomes less valid for higher pressures therefore inhibiting this kind of constrained refinement. However, it allowed us to confirm the expected trend towards a higher coordination number. The Ba-O bond distances show a development towards a [9]-fold and an [8]-fold coordination of the Ba1 and Ba2 atoms, respectively, Fig. 5. This is expressed by a strong decrease of the Ba1-O3 and Ba2-O3 bond distances, respectively. From the evolution of the Ba-O distances, it can be expected that the phase transitions at higher pressures may produce [10]- and even [11]-fold coordinations around the Ba atoms. Such a behavior was shown for barium fluoride, BaF_2,[32–35] which has a similar cation/anion size ratio to the barium hydroxide.

4. Pressure-induced changes of the α-$Ba(OH)_2$ powder-diffraction pattern

The metastable α phase of $Ba(OH)_2$ quenched from high temperature was studied in a pressure range between 5.8 and 11.7 GPa. The starting material was confirmed to be pure α-$Ba(OH)_2$ by exposing the sample in a capillary before it was loaded into the diamond-anvil cell. The high initial pressure resulted from the intrinsic experimental difficulty to close a screw-driven diamond-anvil cell under liquid argon. At the closing pressure of 5.8 GPa the powder diffraction

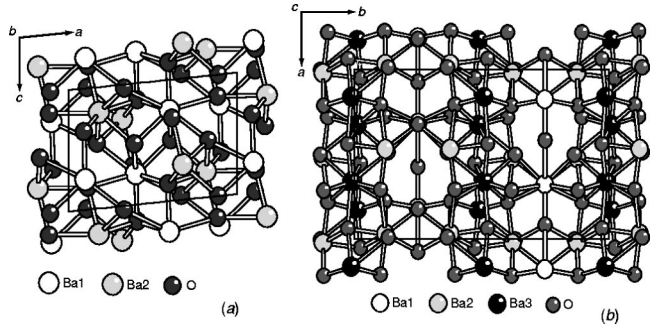

FIG. 2. Crystal structures of (a) β-$Ba(OH)_2$ and (b) α-$Ba(OH)_2$, projected along the *b* and the *c* axes, respectively. Only barium and oxygen atoms are drawn.

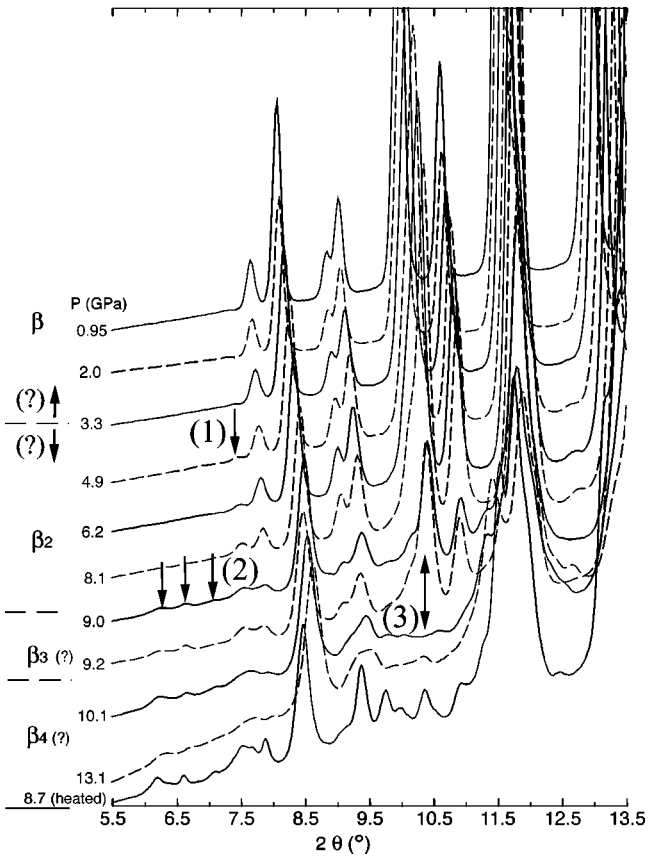

FIG. 3. Selected integrated and scaled powder-diffraction patterns of β-$Ba(OH)_2$ and its high-pressure phases as a function of pressure (GPa) in a selected 2θ range. (1) appearance of a new low-angle peak indicative for the β_2 phase; (2) further weak peaks attributed to a possible β_3 phase; (3) dramatic decrease of intensity of a strong peak around 10.1 GPa (see text for more details).

pattern looks distinctly different from the reference pattern recorded from the capillary, Fig. 6. It cannot be distinguished from the one expected from a mechanical mixture of β_2 and α phases. There are three possible interpretations for this finding: (i) The sample was contaminated with water during the loading process despite the special care paid to keep it under an inert gas atmosphere. This is known to promote the transformation from the α to the β phase.[25] (ii) High pressure promotes the back-transformation of the metastable α phase to the β phase. (iii) High pressure induces the α phase to undergo a phase transition to yet another new phase (α_2) with a powder-diffraction pattern close to a combination of those of the α and β phases. The picture is slightly complicated by the observation of a strong intensity increase of the 6.09 Å ($2\theta = 7.53°$) peak at 9.8 GPa, Fig. 6. This feature has not been observed for the β_2 or β_3 phase in the previous experiment and is therefore attributed to either the α phase or its high-pressure polymorph α_2, which is possibly created during this experiment [hypothesis (iii) above]. The intensity of this peak remains high up to the highest pressure attained and persists also during decompression back to 4.4. GPa. Further pressure release down to 0.3 GPa induces a fundamental rearrangement of peak positions and intensities towards a signal compatible with the β_2 phase. It is only on this pattern that also the prominent low-angle peak around $d = 8.25$ Å ($2\theta = 5.55°$), characteristic for the α phase, disappears, Fig. 6. The observation of a clean β_2 pattern at 0.3 GPa upon decompression is remarkable. It suggests that pressure cycling the metastable α phase creates the β_2 phase at a pressure which in the previous experiment was still well within the stability range of the β phase during compression. The β_2 material generated in such a way remained stable upon subsequent repressurizing up to 8.4 GPa. This indicates a very large hysteresis loop for the β-to-β_2 phase transition.

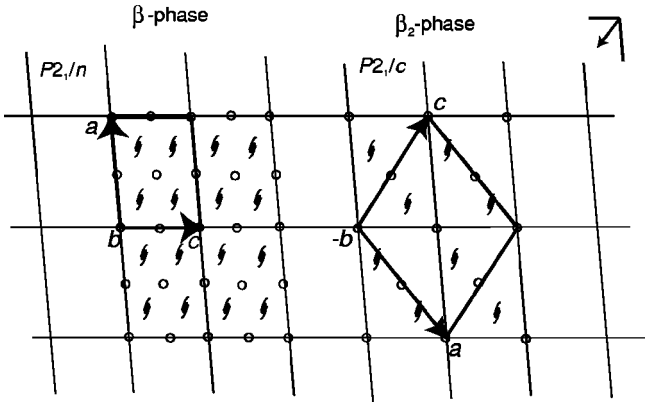

FIG. 4. Geometric relationship between the unit cells and symmetry operations of β- and β_2-$Ba(OH)_2$ projected parallel to the monoclinic axes.

B. Compressibility

The compressional behavior of the β and β_2 phases of $Ba(OH)_2$ is very similar. The P-V curve does not show an observable discontinuity when compressing β-$Ba(OH)_2$, Fig. 7. The pressure steps around 1–2 GPa do also not allow to resolve a discontiunity in the first derivative of the P-V evolution. From this it is also not surprising that the volume of the β_2 unit cell obtained at 0.3 GPa from cycling the α phase lies exactly on the P-V curve of the β phase.

Since we cannot recognize any discontinuity in the first two moments of the volume versus pressure evolution, it is justified to fit the data of both phases with one equation of state (EOS). A third-order Birch-Murnaghan (BM) EOS was fitted to the P-V data between 0.0001 and 8.1 GPa, Fig. 7. The last pressure point of the β_2-phase stability at 8.4 GPa was excluded due to its deviating behavior, which could be caused by the β_2-to-β_3 phase transition, which occurs between 8.4 and 9.0 GPa. The values obtained for the isothermal bulk modulus and its pressure derivative are $K_0 = 35(2)$ GPa and $K' = 12(1)$ at $V_0 = 501.97(2)$ Å^3 ($\chi^2 = 2.9$). The value of K' is unusually high. This is probably because of the subtle β-to-β_2 phase transition around 4 GPa. Therefore, an attempt was done to fit two separate second-order BM EOS's to the P-V data. A first one included data up to 3.3 GPa, i.e., pressures below the expected β-to-β_2 phase transition (excluding the 0.3-GPa pressure point), and a second one included the data from 4.9 to 8.1 GPa. In both fits K' was fixed to a value of 6. This results in

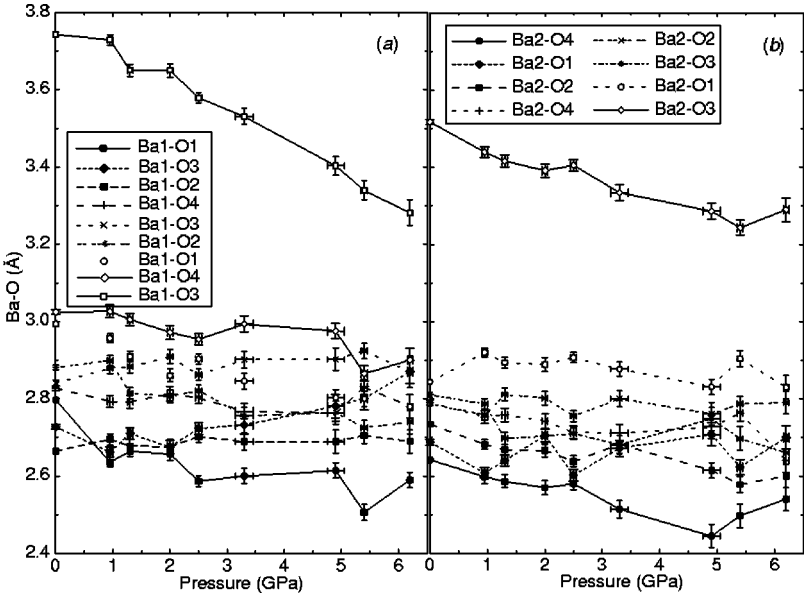

FIG. 5. Barium-oxygen distances (angstrom) of compressed β-Ba$(OH)_2$ as a function of pressure. (a) Ba1-O, (b) Ba2-O.

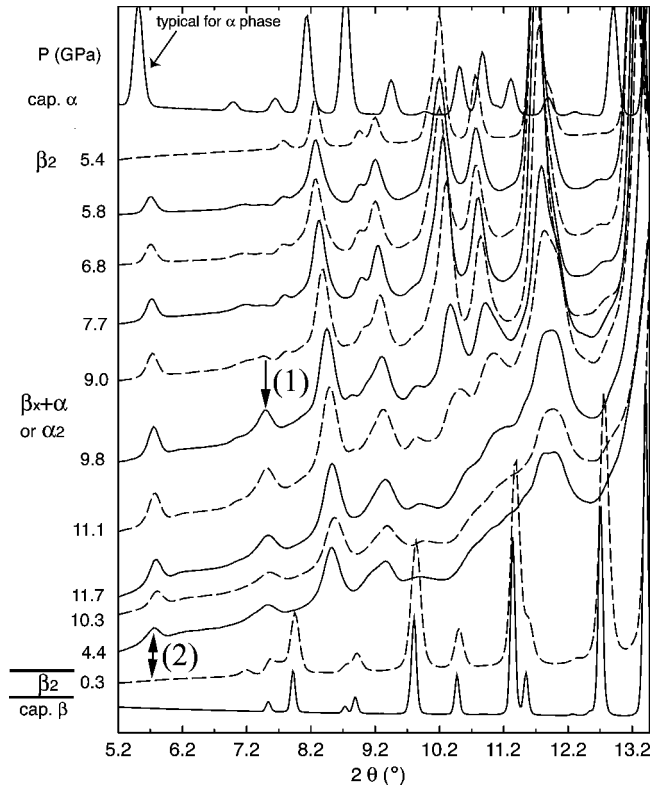

FIG. 6. Selected integrated and scaled powder-diffraction patterns of α-Ba$(OH)_2$ as a function of pressure (GPa) in a selected 2θ range. The patterns are arranged from top to bottom according to the sequence of pressure change. The top two patterns (cap α and β_2 at 5.4 GPa) as well as the bottom pattern (cap β) are reference patterns for comparison. (1) highlights a peak showing a strong intensity increase at 9.8 GPa. (2) points out the disappearance of the α-specific low-angle peak when releasing pressure to 0.3 GPa (see text for more details). Cap. = capillary measurement.

$K_0=40(1)$ GPa, $V_0=501.97(2)$ Å^3 ($\chi^2=5.0$) for the low-pressure range, and $K_0=60(4)$ GPa, $V_0=491(2)$ Å^3 ($\chi^2=3.1$) for the upper-pressure range, respectively. The bulk moduli obtained are very similar to the bulk moduli of other hydroxides, such as Mg$(OH)_2$ [$K_0=54(2)$ GPa, $K'=4.7(2)$],[4] Ca$(OH)_2$ [$K_0=38(2)$ GPa, $K'=5.2(7)$],[8] Mn$(OD)_2$ [$K_0=41(3)$ GPa, $K'=4.7$ (fixed)],[12] Co$(OD)_2$ ($K_0\sim48$ GPa),[12] and Ni$(OD)_2$ ($K_0\sim52$ GPa).[1] A decreasing bulk modulus with increasing cation/anion size ratio is expected due to the softer behavior of the larger cations. The unresolvable discontinuity in the evolution of the volume versus pressure suggests a second-order phase transition. This, however, is in contradiction with a possible large hysteresis loop of the β-β_2 phase transition as discussed above. To resolve this puzzle, more finely stepped data with higher precision are required.

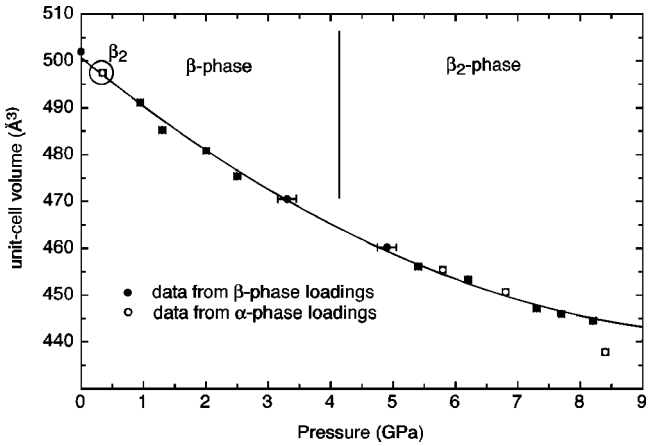

FIG. 7. Reduced unit-cell volumes of β- and β_2-Ba$(OH)_2$ as a function of pressure. The circled β_2 point at 0.3 GPa is retrieved from a pressure-cycled loading of the α phase (see text for more details).

IV. CONCLUSIONS

Our study reveals a rather complex structural behavior for $Ba(OH)_2$ at high pressure. The β phase undergoes at least one, possibly three, pressure-induced phase transitions. The α phase, on the other hand, is destabilized by high pressure, indicated by the formation of the β_2 phase after applying and releasing pressure to α-$Ba(OH)_2$. Within the limits of our powder data, we recognize an (expected) trend towards higher coordination numbers. The compressibility of the β phase does not show any discernible discontinuity at the structurally observed phase change. The values for the bulk moduli are in line with the compressibility of other hydroxides.

A similar complex phase diagram at high pressure is observed for BaF_2. In view of the fact that at high pressure the structural complexity of both hydroxides and fluorides (where no hydrogen bonds can be formed) gains in complexity, we postulate that hydrogen bonding plays a secondary role in the pressure-induced phase transitions. The primary influence is suggested to be the size ratio between cations and anions. This hypothesis is corroborated by the similarity of the high-pressure phase of compounds with small cations to the ambient condition structure of hydroxides with large cations [e.g., $Ca(OH)_2$ and $Sr(OH)_2$]. Furthermore, pressure-induced phase transitions are generally accompanied by an increase of the coordination number of the cations rather than a redistribution of hydrogen bonds. The nature of the newly formed high-pressure phases, however, is influenced by hydrogen bonds. Hydrogen atoms allow for additional structural flexibility as the asymmetric hydrogen bonds help to redistribute electrons within the structure. By this way, they enable to balance bond-valence requirements imposed on the framework atoms through the volume compression.[36] The significant influence of hydrogen bonds on the structural conformations can be shown when comparing the alkaline-earth hydroxides with their fluoride equivalents. The crystal structures of MgF_2 (rutile structure), CaF_2, SrF_2, and BaF_2 (fluorite structure) are completely different from the ones of the respective hydroxyl equivalents, although the ionic radii of OH^- and F^- are similar.

ACKNOWLEDGMENTS

Experiment 01-02-257 was supported by the Swiss-Norwegian Beamline. The authors thank the staff of the ID30 high-pressure beamline and Dr. H. Mueller for the use of their laboratories. A. Friedrich was financially supported by the Swiss National Science Foundation (credit 21-052682.97 to M. Kunz).

*Present address: Institut für Mineralogie, Abt. Kristallographie, J. W. Goethe-Universität, Senckenberganlage 30, D-60054 Frankfurt am Main, Germany. Electronic address: friedrich@kristall.erdw.ethz.ch

†Present address: Department of Earth Sciences, University of Basel, Bernoullistrasse 30, CH-4056 Basel, Switzerland and Naturhistorisches Museum, Augustinergasse 2, CH-4001 Basel, Switzerland.

‡Present address: Mineralogisches Institut, Universität Heidelberg, Im Neuenheimer Feld 236, D-69120 Heidelberg, Deutschland.

[1] J.B. Parise, H. Cox, H. Kagi, R. Li, W. Marshall, J.S. Loveday, and S. Klotz, Rev. High Pressure Sci. Technol. **7**, 211 (1998).

[2] M.B. Kruger, Q. Williams, and R. Jeanloz, J. Chem. Phys. **91**, 5910 (1989).

[3] T.S. Duffy, T.J. Ahrens, and M.A. Lange, J. Geophys. Res. [Solid Earth] **96**, 14 319 (1991).

[4] Y. Fei and H.-K. Mao, J. Geophys. Res. [Solid Earth] **98**, 11 875 (1993).

[5] T.S. Duffy, J. Shu, H.-K. Mao, and R.J. Hemley, Phys. Chem. Miner. **22**, 277 (1995).

[6] J.B. Parise, K. Leinenweber, D.J. Weidner, K. Tan, and R.B. VonDreele, Am. Mineral. **79**, 193 (1994).

[7] M. Catti, G. Ferraris, S. Hull, and A. Pavese, Phys. Chem. Miner. **22**, 200 (1995).

[8] C. Meade and R. Jeanloz, Geophys. Res. Lett. **17**, 1157 (1990).

[9] C. Meade, R. Jeanloz, and R. J. Hemley, in *High-Pressure Research: Application to Earth and Planetary Sciences*, edited by Y. Syono and M. H. Manghnani (Terra, Washington, D.C., 1992), p. 485.

[10] X. Xia, D.J. Weidner, and H. Zhao, Am. Mineral. **83**, 68 (1998).

[11] J.H. Nguyen, M.B. Kruger, and R. Jeanloz, Phys. Rev. B **49**, 3734 (1994).

[12] J.B. Parise, B. Theroux, R. Li, J.S. Loveday, W.G. Marshall, and S. Klotz, Phys. Chem. Miner. **25**, 130 (1998).

[13] T.S. Duffy, C. Meade, Y.W. Fei, H.K. Mao, and R.J. Hemley, Am. Mineral. **80**, 222 (1995).

[14] K. Leinenweber, National Synchrotron Light Source, Annual Report, 1993 (unpublished).

[15] M. Kunz, K. Leinenweber, J.B. Parise, T.-C. Wu, W.A. Bassett, K. Brister, D.J. Weidner, M.T. Vaughan, and Y. Wang, High Press. Res. **14**, 311 (1996).

[16] A. Pavese, M. Catti, G. Ferraris, and S. Hull, Phys. Chem. Miner. **24**, 85 (1997).

[17] K. Leinenweber, U. Schuelke, and M. O'Keeffe, J. Solid State Chem. **132**, 267 (1997).

[18] B. Winkler, V. Milman, and M. Kunz, Eur. J. Mineral. **14**, 557 (2002).

[19] D.E. Partin and M. O'Keeffe, J. Solid State Chem. **119**, 157 (1995).

[20] A.E. Ringwood and A. Major, Earth Planet. Sci. Lett. **2**, 130 (1967).

[21] E.H.P. Cordfunke, A.S. Booji, R.J.M. Konings, R.R. van der Laan, V.M. Smit-Groen, and P. van Vlaanderen, Thermochim. Acta **273**, 1 (1996).

[22] H. Lüke, Ph.D. thesis, Universität Karlsruhe, 1973.

[23] W. Denzinger, Ph.D. thesis, Universität Karlsruhe, 1997.

[24] H. Bärnighausen, W. Denzinger, and T. Zeiske, Z. Kristallogr. Suppl. **12**, 212 (1997).

[25] A. Friedrich, M. Kunz, and E. Suard, Acta Crystallogr., Sect. B: Struct. Sci. **57**, 747 (2001).

[26] R. Miletich, D. R. Allan, and W. F. Kuhs, in *High-Temperature and High-Pressure Crystal Chemistry, Mineralogical Society of America Reviews in Mineralogy and Geochemistry*, edited by R. M. Hazen and R. T. Downs (The Mineralogical Society of

America and the Geochemical Society, Washington, D.C., 2000), Vol. 41, p. 445.
[27] A. Hammersley, computer code FIT2D, version 10.27, reference manual, European Synchrotron Radiation Facility, Grenoble, France, 1998.
[28] A. C. Larson and R. B. Von Dreele, Los Alamos Laboratory Report No. LA-UR-86-748 (Rev. 9/2/94) (unpublished), p. 86.
[29] P.-E. Werner, L. Eriksson, and M. Westdahl, J. Appl. Crystallogr. **18**, 367 (1985).
[30] J.W. Visser, J. Appl. Crystallogr. **2**, 89 (1969).
[31] D. Louër, NIST Spec. Publ. **846**, 92 (1992).
[32] J.M. Léger, A.M. Redon, and C. Chateau, Phys. Chem. Miner. **17**, 161 (1990).
[33] J.M. Léger, J. Haines, A. Atouf, O. Schulte, and S. Hull, Phys. Rev. B **52**, 13 247 (1995).
[34] J.M. Léger, J. Haines, and A. Atouf, Phys. Rev. B **51**, 3902 (1995).
[35] J. Haines, J.M. Léger, and O. Schulte, Phys. Rev. B **57**, 7551 (1998).
[36] I.D. Brown, Acta Crystallogr., Sect. B: Struct. Sci. **48**, 553 (1992).